

Communication

# Nonlinear Dynamics of Mid-Infrared Interband Cascade Lasers Subject to Variable-Aperture Optical Feedback

Maorong Zhao <sup>1,2,3</sup>, Guangqiong Xia <sup>1,2</sup> , Ke Yang <sup>4,5</sup>, Shuman Liu <sup>4,5</sup> , Junqi Liu <sup>4,5</sup>, Qiupin Wang <sup>1,2</sup>, Jianglong Liu <sup>1,2</sup> and Zhengmao Wu <sup>1,2,\*</sup> 

- <sup>1</sup> School of Physical Science and Technology, Southwest University, Chongqing 400715, China; zhaomaorong@email.swu.edu.cn (M.Z.); gqxia@swu.edu.cn (G.X.); w1562067325@email.swu.edu.cn (Q.W.); l2439326799@email.swu.edu.cn (J.L.)
- <sup>2</sup> Chongqing Key Laboratory of Micro & Nano Structure Optoelectronics, Southwest University, Chongqing 400715, China
- <sup>3</sup> School of Information, Southwest Petroleum University, Nanchong 637001, China
- <sup>4</sup> Key Laboratory of Semiconductor Materials Science, Beijing Key Laboratory of Low Dimensional Semiconductor Materials and Devices, Institute of Semiconductors, Chinese Academy of Sciences, P.O. Box 912, Beijing 100083, China; jqliu@semi.ac.cn (J.L.); yangke17@semi.ac.cn (K.Y.); liusm@semi.ac.cn (S.L.)
- <sup>5</sup> Center of Materials Science and Optoelectronics Engineering, University of Chinese Academy of Sciences, Beijing 100049, China
- \* Correspondence: zmwu@swu.edu.cn

**Abstract:** In this work, we experimentally investigate the nonlinear dynamics of an interband cascade laser (ICL) under variable-aperture optical feedback implemented by a gold mirror combining with a ring-actuated iris diaphragm (RAID). By continuously varying the diameter of RAID ( $D_R$ ), the evolution of the dynamical state of ICL with the aperture of the optical feedback can be inspected. The characteristics of each dynamical state are characterized by time series, power spectra, phase portraits, and Lyapunov exponents. The results show that, with the decrease of  $D_R$ , the dynamical state of the ICL under variable-aperture optical feedback presents an evolution from complex, simple to stable. Diverse dynamical states including period one state (P1), period two state (P2), multi-period state (MP), quasi-period state (QP), low-frequency fluctuation (LFF), chaotic state (C), and hyperchaos have been observed. Through mapping the evolution of dynamical states with  $D_R$  for the ICL biased at different currents, different evolved routes of the dynamical states are revealed.

**Keywords:** interband cascade laser (ICL); nonlinear dynamics; optical feedback



**Citation:** Zhao, M.; Xia, G.; Yang, K.; Liu, S.; Liu, J.; Wang, Q.; Liu, J.; Wu, Z. Nonlinear Dynamics of Mid-Infrared Interband Cascade Lasers Subject to Variable-Aperture Optical Feedback. *Photonics* **2022**, *9*, 410. <https://doi.org/10.3390/photonics9060410>

Received: 17 May 2022

Accepted: 9 June 2022

Published: 10 June 2022

**Publisher's Note:** MDPI stays neutral with regard to jurisdictional claims in published maps and institutional affiliations.



**Copyright:** © 2022 by the authors. Licensee MDPI, Basel, Switzerland. This article is an open access article distributed under the terms and conditions of the Creative Commons Attribution (CC BY) license (<https://creativecommons.org/licenses/by/4.0/>).

## 1. Introduction

Interband cascade laser (ICL) is a kind of important mid-infrared semiconductor lasers, where the advantages of interband optical transition from quantum well lasers (QWLs) and the electron transport via the cascading stages from quantum cascade lasers (QCLs) are combined in the ICL [1,2]. Unlike ordinary QCLs, ICL is based on the interband transition of type-II quantum wells for emitting light, and its carrier lifetime is on the order of sub-nanoseconds [2–4]. ICL typically has five to ten cascading gain stages in its active region for enhancing the total gain. The power consumption of ICL is 1–2 orders of magnitude lower than that of mid-infrared QCL, allowing for battery-powered operation [5,6]. GaSb-based ICLs can oscillate within a wavelength range from 3  $\mu\text{m}$  to 6  $\mu\text{m}$  [2,3], while InAs-based ICLs can oscillate at a wavelength beyond 10  $\mu\text{m}$  [7]. As a result, ICLs can be used for gas sensing [8,9] and free-space optical (FSO) communication [10] due to the unique mid-infrared spectral range.

Previous research has demonstrated that near-infrared semiconductor lasers exhibit a variety of dynamical states under external perturbations including optical injection, optical feedback, or optoelectronic feedback [11–17], which is of particular interest in many

applications, including photonic microwave signal generation [18–20], random bit generation [21,22], secure communications [23,24], high performance radar, and lidar [25–27], as well as photonic reservoir computing [28]. For mid-infrared QCLs, related theoretical and experimental investigations on the nonlinear dynamics and their applications have been explored, and the results demonstrate that, compared with near-infrared semiconductor lasers, QCLs are less sensitive to optical feedback [29,30]. Under some special operation conditions, optical feedback QCLs can exhibit low-frequency fluctuations [31,32]. As for mid-infrared ICLs, relevant theoretical investigation predicts that an ICL under optical feedback can exhibit chaotic state [33], which has been experimentally demonstrated very recently [34].

For near-infrared semiconductor laser, the optical feedback with variable feedback ratio is relatively easy to be implemented by combining a mirror with a neutral density filter (NDF). However, for mid-infrared waveband, currently commercial NDF cannot provide continuously variable attenuation rate. Therefore, in order to build a feedback system with continuous change of feedback strength, the feedback loop based on polaroid has been proposed and demonstrated in mid-infrared external cavity QCLs [29–32] and ICLs [34]. Through changing the polarized state of the feedback light, the feedback ratio can be adjusted.

In this work, we propose a novel scheme to establish a feedback loop implemented via a ring-actuated iris diaphragm (RAID) combining with a mirror. Through varying the diameter ( $D_R$ ) of RAID, the aperture of feedback beam can be adjusted. As a result, we investigate the nonlinear dynamics of an ICL via the time series, power spectra, phase portraits, and Lyapunov exponents. Moreover, the dynamical state evolution of the ICL with  $D_R$  is also explored.

## 2. Experimental Setup

Figure 1 shows the schematic diagram of the experimental setup. The interband cascade laser (ICL) utilized in this experiment is a Fabry–Perot laser operating at the wave band of 3.3  $\mu\text{m}$ , which is grown on GaSb substrate by solid source molecular beam epitaxy. The ICL is composed of five cascading stages of W-shaped active regions formed by InAs/GaInSb type-II quantum wells, and two cleavage planes form the resonant cavity. The ridge width and cavity length of the ICL are 20  $\mu\text{m}$  and 2.0 mm, respectively. The purpose of such a relatively broad area laser structure is to obtain high power. An aspheric lens is encapsulated in the laser to collimate the emission light. The ICL is driven by a high stability and low-noise current-temperature controller (ILX-Lightwave, LDC-3724C). During the total experimental processes, the temperature is stabilized at 20.15  $^{\circ}\text{C}$ . The laser beam output from the ICL is divided into two parts by a 75:25 beam splitter (BS). The 75%-part is reflected by a plane gold mirror and then fed back to the ICL. The gold mirror is placed 21.6 cm away from the ICL. A ring-actuated iris diaphragm (RAID) is added into the feedback loop for adjusting the aperture of optical feedback, and its diameter ( $D_R$ ) can be adjusted from 1.0 to 8.0 mm. The 25%-part is converted into electronic signal by a fast HgCdTe photodetector (PD, Vigo PVI-4TE-5, 525 MHz bandwidth), and then is sent to the detected system. The time series and electrical spectra are recorded by a digital oscilloscope with a sampling rate of 20 GS/s (OSC, Agilent DSO9254A with 2.5 GHz bandwidth) and an electrical spectrum analyzer (ESA, Agilent E4407B with 26.5 GHz bandwidth), respectively.

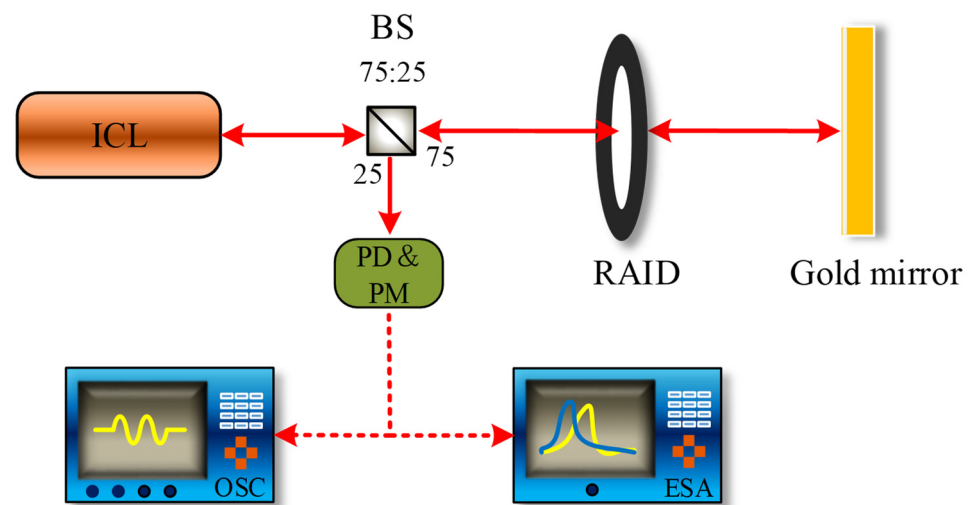


**Figure 1.** Schematic diagram of the experimental setup. ICL: Interband cascade laser, BS: Beam splitter, RAID: Ring-actuated iris diaphragm, PM: Power meter, PD: Photodetector, OSC: Oscilloscope, ESA: Electrical spectrum analyzer. Solid line: optical path, dashed line: microwave path.

### 3. Results

Figure 2 shows the measured power-current characteristic of the ICL at free-running (blue) and subject to variable-aperture optical feedback under  $D_R = 4.0$  mm (red). Here, the output power of the ICL is monitored by a power meter (PM) at the 25% output port of BS. As shown in this diagram, the free-running ICL exhibits a threshold current  $I_{th}$  of 74.50 mA. After introducing variable-aperture optical feedback under  $D_R = 4.0$  mm, the threshold current is decreased to 64.80 mA, and, meanwhile, the output power is significantly enhanced. Further experimental results show that the power-current characteristic of the ICL is not affected by the variation of  $D_R$  under the case that  $D_R$  is beyond 3.7 mm. In other words, under this experimental condition the size of the optical beam is about 3.7 mm. Therefore, the red curve in Figure 2 also corresponds to the case that the RAID is removed. In the following discussion, the value of  $D_R$  is set to no more than 3.7 mm.

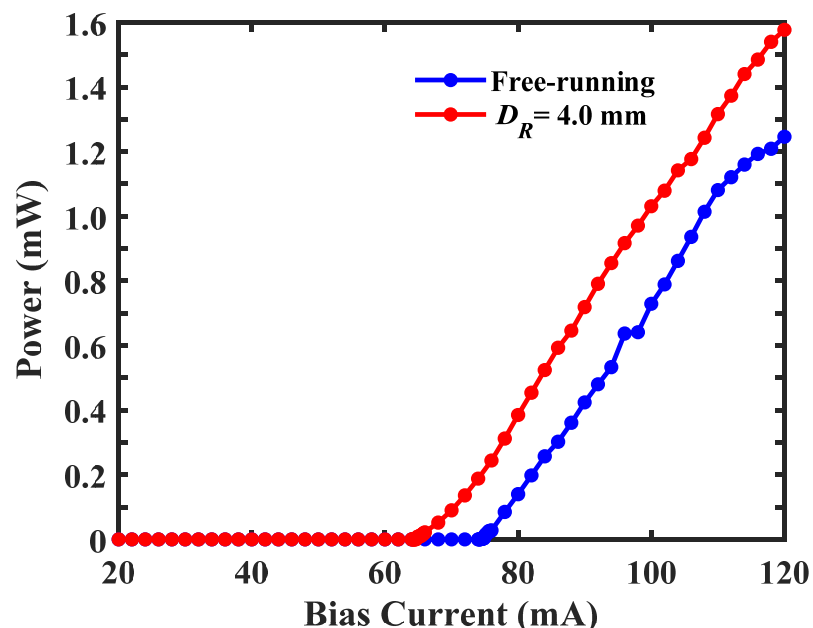


**Figure 2.** Power-current characteristic of the ICL at free-running (blue) and subject to variable-aperture optical feedback under  $D_R = 4.0$  mm (red).

First, we fix the bias current at a relatively low level ( $I = 86.00$  mA) and inspect the dynamical states of the ICL under variable-aperture optical feedback. Figure 3 displays the time series (first column), power spectra (second column), and corresponding phase portraits (third column) for some typical dynamical states of the ICL subject to variable-aperture optical feedback under different  $D_R$ . For  $D_R = 3.7$  mm, as mentioned above, the feedback optical beam does not be limited by the RAID. Under this case, a slowly-varying envelope can be observed from the time series (in Figure 3(a1)), two or more incommensurate frequencies exist in the power spectrum (in Figure 3(b1)), and the phase portrait (in Figure 3(c1)) is characterized by a torus. Thus, this dynamical state of the ICL corresponds to a quasi-periodic state (QP). For  $D_R = 3.0$  mm (as shown in Figure 3(a2,b2,c2)), the time series behaves as a periodic oscillation whose fundamental frequency is about 259.4 MHz from the power spectrum, and the phase portrait shows a limited cycle feature. Therefore, it can be judged that the ICL operates at a period one state (P1). For  $D_R = 2.6$  mm (as shown in Figure 3(a3,b2,c3)), two peak intensities in the time series can be clearly observed, both sub-harmonic frequency (about 127.4 MHz) and fundamental frequency (about 256.4 MHz) appear in the power spectrum, and the corresponding phase portrait possesses two loops that are intertwined together. All these features mean that the dynamical state of the ICL is a period two state (P2). For  $D_R = 2.3$  mm (as shown in Figure 3(a4,b4,c4)), random intensity oscillation can be seen from the time series, the corresponding power spectrum covers a broad frequency range, and the phase portrait shows a widely scattered distribution over a large area. As a result, the ICL exhibits a chaotic state (C). Finally, for  $D_R = 1.0$  mm, which is the minimum diameter of the RAID, the time series (Figure 3(a5)) has some tiny fluctuations, mainly caused by the system noise. Accordingly, the power spectrum (Figure 3(b5)) almost coincides with the noise floor, and the phase portrait (Figure 3(c5)) shrinks as a small spot. Therefore, the dynamical state of the ICL is a stable state (S). In short, an evolution route of QP-P1-P2-C-S is presented under  $I = 86.00$  mA through gradually decreasing  $D_R$ , and the reason may be explained as follows. After introducing a RAID into the feedback loop, the edge portion of the beam beyond the diameter of RAID will be blocked. For a relatively large value of  $D_R$ , the fundamental transverse mode is almost unlimited and can be fed back into the ICL. However, the higher-order transverse mode is limited by the RAID, which results in a decrease in the feedback. As a result, with the decrease in  $D_R$ , the fundamental transverse mode can be driven into a more complex dynamical state. However, if  $D_R$  is decreased below the size of fundamental transverse mode, the feedback strength of the fundamental transverse mode will be weakened with the decrease of  $D_R$ , and then the ICL will operate at a steady state for too small  $D_R$ .

Next, we fix the bias current at a relatively high level ( $I = 96.00$  mA) and examine the influence of  $D_R$  on the dynamical states of the ICL, and the corresponding results are presented in Figure 4. For  $D_R = 3.7$  mm (Figure 4(a1,b1,c1)), similar dynamical characteristics with Figure 3(a1,b1,c1) can be observed, and the dynamical state is QP. When  $D_R$  is decreased to 3.3 mm (Figure 4(a2,b2,c2)), the dynamical state of the ICL is P1 with a fundamental frequency of 239.9 MHz. Further decreasing  $D_R$  to 2.8 mm (Figure 4(a3,b3,c3)), the dynamical features of the ICL are similar to that in Figure 3(a3,b3,c3), both the fundamental frequency (about 237.9 MHz) and its sub-harmonic frequency (about 118.9 MHz) present clearly in the power spectrum, and then the dynamics can be identified as P2. For  $D_R = 2.7$  mm (Figure 4(a4,b4,c4)), the time series shows multiple different peaks, multiple frequency components appear upon the power spectrum, and the phase portrait shows the overlap alternation of multiple loops. Therefore, the ICL presents a multi-period state (MP). For  $D_R = 2.5$  mm (Figure 4(a5,b5,c5)), the time series fluctuates dramatically, the corresponding power spectrum continuously covers a broad frequency range, and the phase portrait shows a widely scattered distribution over a large area. Under these circumstances, it can be determined that the ICL operates at a chaotic state (C). Furthermore, if  $D_R$  is decreased to 1.6 mm (Figure 4(a6,b6,c6)), the time series exhibits a sudden power dropout with a following gradual power recovery. In addition, the time series raises the low-frequency noise for frequency below about 20 MHz in the power spectrum, and the phase portrait

shows a cluster sited around  $-0.13$  to  $0.06$  V. All these features indicate that the ICL exhibits a low-frequency fluctuation (LFF). In further decreasing  $D_R$  to  $1.0$  mm (Figure 4(a7,b7,c7)), the ICL shows an S state. In a word, with the decrease of  $D_R$  from  $3.7$  mm to  $1.0$  mm, the ICL shows rich nonlinear dynamical states followed a route of QP-P1-P2-MP-C-LFF-S.

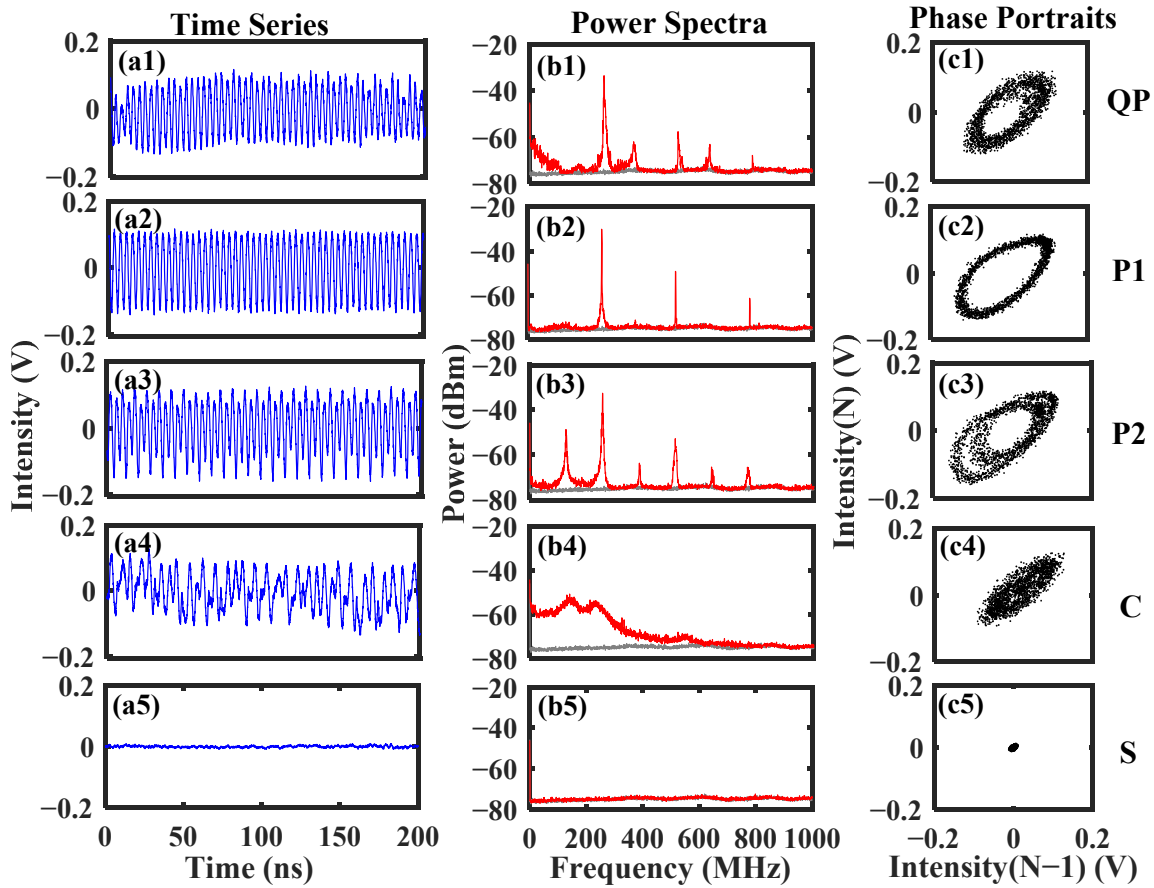


**Figure 3.** Time series (a1–a5), power spectra (b1–b5), and corresponding phase portraits (c1–c5) for some typical dynamical states of the ICL biased at  $I = 86.00$  mA under variable-aperture optical feedback with  $D_R$  of  $3.7$  mm (row 1),  $3.0$  mm (row 2),  $2.6$  mm (row 3),  $2.3$  mm (row 4), and  $1.0$  mm (row 5). The gray lines in the power spectra denote the noise floor. QP: quasi-period state; P1: period one state; P2: period two state; C: chaotic state; S: stable state.

The largest Lyapunov exponent (LLE), which describes the divergence rate of nearby attractor trajectories, is an effective method to determine the dynamical state [35,36]. A chaotic state at least possesses one positive Lyapunov exponent [37,38]. Based on the time series, we have calculated the evolution of LLE with  $D_R$  under  $I = 96.00$  mA, and the results are given in Figure 5a. As shown in Figure 5a, when  $D_R$  is decreased from  $3.7$  mm to  $2.6$  mm, the ICL exhibits different states of QP-P1-P2-MP, and the values of LLE are nearly zero. When further decreasing  $D_R$ , the ICL is driven into C state, and the LLE arrives at its maximum value of  $1.69 \text{ ns}^{-1}$  under  $D_R = 2.5$  mm. For the case that  $D_R$  is decreased from  $2.3$  mm to  $1.6$  mm, the ICL exhibits LFF, and the LLEs are  $0.93 \text{ ns}^{-1}$ ,  $0.52 \text{ ns}^{-1}$ , respectively. Figure 5b shows the corresponding Lyapunov exponent spectrum when the LLE arrives at the maximum value of  $1.69 \text{ ns}^{-1}$ . From this diagram, it can be seen that five largest Lyapunov exponents are  $1.62, 0.94, 0.37, -0.06,$  and  $-0.61 \text{ ns}^{-1}$ . As a result, there exist three positive Lyapunov exponents, which demonstrates that the output of ICL is hyperchaos [39].

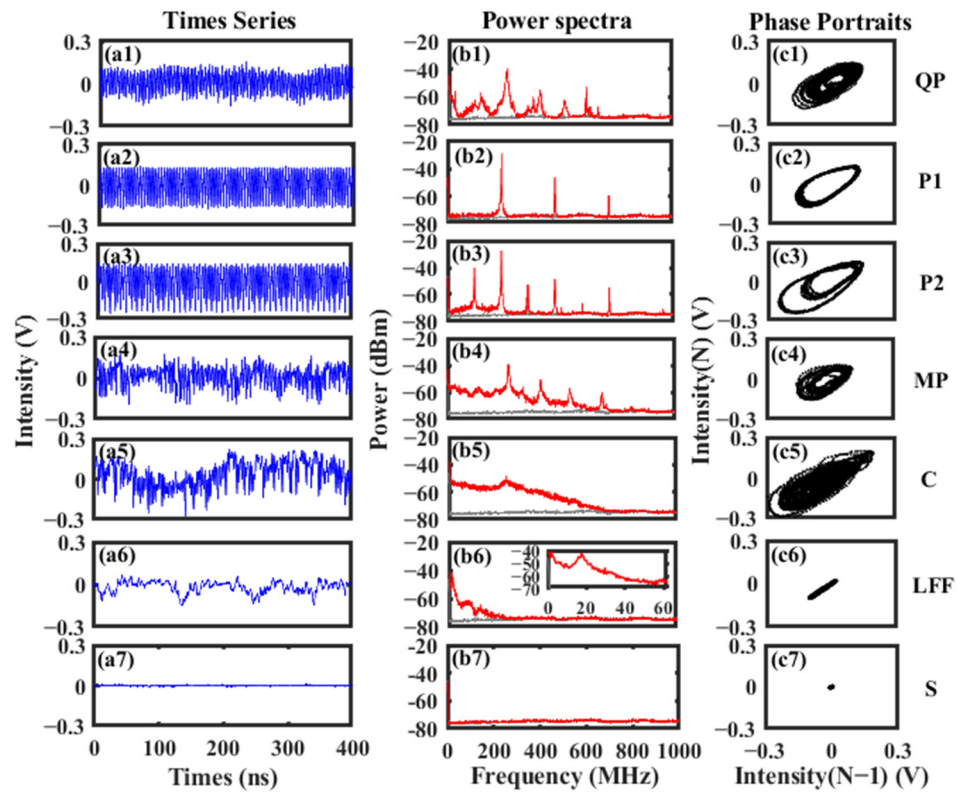


**Figure 4.** Time series (a1–a5), power spectra (b1–b5), and corresponding phase portraits (c1–c5) for some typical dynamical states of the ICL biased at  $I = 96.00$  mA subject to variable-aperture optical feedback with  $D_R$  of 3.7 mm (row 1), 3.3 mm (row 2), 2.8 mm (row 3), 2.7 mm (row 4), 2.5 mm (row 5), 1.6 mm (row 6), and 1.0 mm (row 7). The gray lines in the power spectra denote the noise floor. MP: multi-period state; LFF: low-frequency fluctuation.

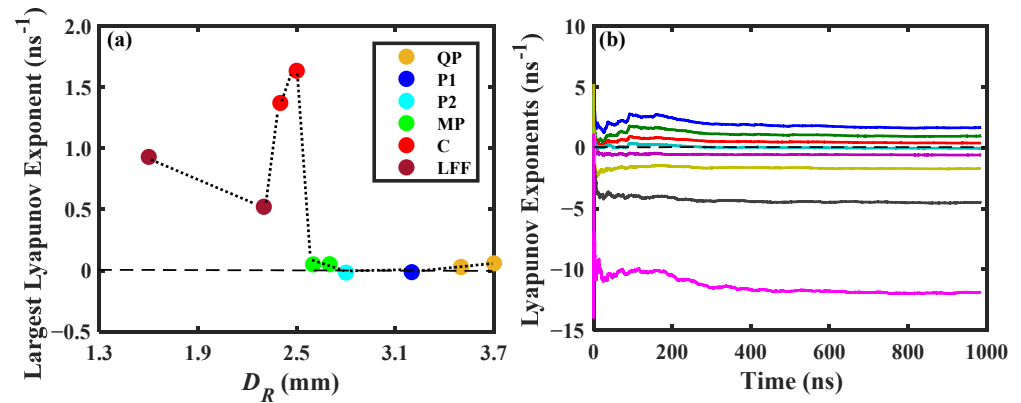


**Figure 5.** (a) Largest Lyapunov exponent as a function of  $D_R$  under the ICL biased at  $I = 96.00$  mA, and (b) Lyapunov exponent spectrum of the chaotic output obtained under  $D_R = 2.5$  mm. For the calculated spectrum, the curves converge to values  $1.62 \text{ ns}^{-1}$ ,  $0.94 \text{ ns}^{-1}$ ,  $0.37 \text{ ns}^{-1}$ ,  $-0.06 \text{ ns}^{-1}$ ,  $-0.61 \text{ ns}^{-1}$ ,  $-1.75 \text{ ns}^{-1}$ ,  $-4.53 \text{ ns}^{-1}$ , and  $-11.89 \text{ ns}^{-1}$  from the top down.

The above results reveal that the bias current  $I$  and the diameter  $D_R$  of RAID are two key parameters to seriously affect the dynamical state of the ICL. Finally, a two-dimensional map of the dynamical evolutions of the ICL under variable-aperture optical feedback in the parameter space of  $I$  and  $D_R$  is integrated in Figure 6, where the bias current varies from 80.00 mA to 96.00 mA with a step of 2.00 mA and the diameter of RAID is varied from 1.0 to 3.7 mm. From this diagram, one can see that a large bias current is helpful for that the ICL presents rich nonlinear dynamical states. For the ICL biased at 80.00 mA, the dynamical states only involve P1 and stable state. If the bias current of ICL is increased to

86.00 mA, with the continuous decrease of  $D_R$ , the ICL can be entered into C state via a route of QP-P1-P2-C. For a larger bias current of the ICL, the evolution of dynamical state with  $D_R$  follows a route of QP-P1-P2-MP-C-LFF-S.

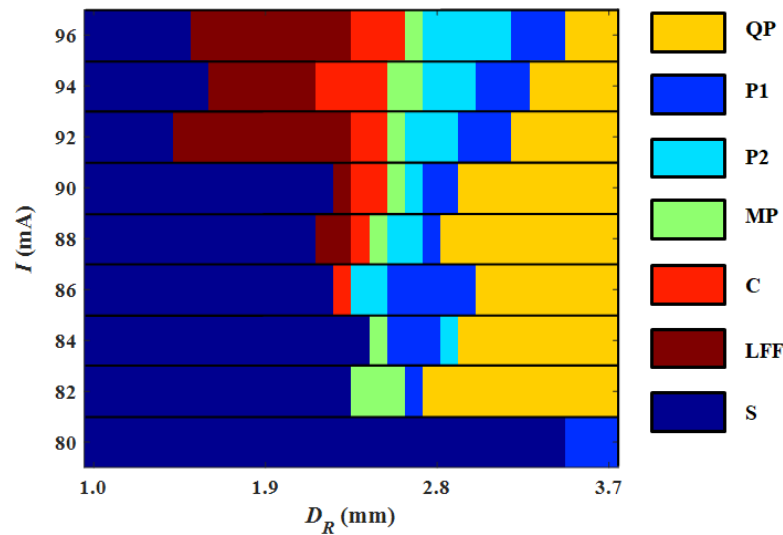


**Figure 6.** Mapping of the dynamical states of the ICL under variable-aperture optical feedback in the parameter space of  $I$  and  $D_R$ . Different color blocks correspond to different dynamical states.

#### 4. Discussion

In this work, based on a ring-actuated iris diaphragm (RAID) combining with a mirror, a novel feedback scheme is proposed for driving an ICL into different dynamical states, which have application prospects in free-space optical communication and sensing, optical generation of microwave, radar and lidar, etc. For such a feedback scheme, the variation of feedback strength is realized through changing the transverse field distribution implemented by adjusting the aperture of RAID. Therefore, compared to the feedback loop based on polarizers [29–32,34], such a feedback scheme is more simple and easily implemented.

Additionally, as proved in Ref. [40], the beam shaping with optical feedback in QCLs is a flexible solution to obtain high-quality mid-infrared sources by controlling the filamentation. Due to a similar principle, it can be predicted that through introducing such a feedback scheme into ICLs, high-quality mid-infrared sources can also be obtained. As a result, we will pay attention to this issue in our further research.

#### 5. Conclusions

In summary, the nonlinear dynamics of an interband cascade laser (ICL) under variable-aperture optical feedback are experimentally investigated, where the variable-aperture optical feedback is implemented by a gold mirror combining with a ring-actuated iris diaphragm (RAID). Via the time series, power spectra, phase portraits, and largest Lyapunov exponent (LLE), the dynamical states of the ICL under variable-aperture optical feedback can be determined, and various dynamical states, including period one state (P1), period two state (P2), multi-period state (MP), quasi-period state (QP), low-frequency fluctuation (LFF), chaotic state (C), and hyperchaos, have been observed. Through mapping the dynamical states in a parameter space of the bias current ( $I$ ) of ICL and the diameter ( $D_R$ ) of RAID, different evolution routes of dynamical state are revealed. Due to the unique virtue of relatively easy implementation, we hope that this work can offer an effective way to control ICL operating at an expected dynamical state for some special scenarios.

**Author Contributions:** Conceptualization, M.Z. and G.X.; methodology, M.Z.; validation, M.Z., G.X. and Z.W.; investigation, M.Z. and K.Y.; resources, G.X., S.L. and J.L. (Junqi Liu); data curation, Q.W. and J.L. (Jianglong Liu); writing—original draft preparation, M.Z.; writing—review and editing, G.X. and Z.W.; visualization, M.Z.; supervision, Z.W.; project administration, G.X. All authors have read and agreed to the published version of the manuscript.

**Funding:** This research was funded by National Natural Science Foundation of China (61875167, 61790583 and 61835011) and Bureau of Science and Technology of Nanchong City (19SXHZ0021).

**Data Availability Statement:** Not applicable.

**Conflicts of Interest:** The authors declare no conflict of interest.

## References

1. Meyer, J.; Bewley, W.; Canedy, C.; Kim, C.; Kim, M.; Merritt, C.; Vurgaftman, I. The interband cascade lasers. *Photonics* **2020**, *7*, 75. [[CrossRef](#)]
2. Ning, C.; Yu, T.; Liu, S.M.; Zhang, J.C.; Wang, L.J.; Liu, J.Q.; Zhuo, N.; Zhai, S.Q.; Li, Y.; Liu, F.Q. Interband cascade lasers with short electron injector. *Chin. Opt. Lett.* **2022**, *20*, 022501. [[CrossRef](#)]
3. Vurgaftman, I.; Bewley, W.W.; Canedy, C.L.; Kim, C.S.; Kim, M.; Merritt, C.D.; Abell, J.; Meyer, J.R. Interband cascade lasers with low threshold powers and high output powers. *IEEE J. Sel. Top. Quantum Electron.* **2013**, *19*, 1200210. [[CrossRef](#)]
4. Didier, P.; Spitz, O.; Cerutti, L.; Diaz-Thomas, D.A.; Baranov, A.N.; Carras, M.; Grillot, F. Relative intensity noise and intrinsic properties of RF mounted interband cascade laser. *Appl. Phys. Lett.* **2021**, *119*, 171107. [[CrossRef](#)]
5. Vurgaftman, I.; Bewley, W.W.; Canedy, C.L.; Kim, C.S.; Kim, M.; Merritt, C.D.; Abell, J.; Lindle, J.R.; Meyer, J.R. Rebalancing of internally generated carriers for mid-infrared interband cascade lasers with very low power consumption. *Nat. Commun.* **2011**, *2*, 585. [[CrossRef](#)] [[PubMed](#)]
6. Bradshaw, J.L.; Yang, R.Q.; Bruno, J.D.; Pham, J.T.; Wortman, D.E. High-efficiency interband cascade lasers with peak power exceeding 4 W/facet. *Appl. Phys. Lett.* **1999**, *75*, 2362–2364. [[CrossRef](#)]
7. Tian, Z.; Li, L.; Ye, H.; Yang, R.Q.; Mishima, T.D.; Santos, M.B.; Johnson, M.B. InAs-based interband cascade lasers with emission wavelength at 10.4  $\mu\text{m}$ . *Electron. Lett.* **2012**, *48*, 113–114. [[CrossRef](#)]
8. Liu, Z.W.; Zheng, C.T.; Chen, C.; Li, Y.F.; Xie, H.T.; Ren, Q.; Wang, Y.D.; Tittel, F.K. ICL-based mid-infrared carbon dioxide sensor system for deep-sea natural gas hydrate exploration. *Opt. Express* **2019**, *27*, 5598–5609. [[CrossRef](#)]
9. Dong, L.; Li, C.G.; Sanchez, N.P.; Gluszek, A.K.; Griffin, R.J.; Tittel, F.K. Compact CH<sub>4</sub> sensor system based on a continuous-wave, low power consumption, room temperature interband cascade laser. *Appl. Phys. Lett.* **2016**, *108*, 011106. [[CrossRef](#)]
10. Soibel, A.; Wright, M.W.; Farr, W.H.; Keo, S.A.; Hill, C.J.; Yang, R.Q.; Liu, H.C. Midinfrared interband cascade laser for free space optical communication. *IEEE Photonics Technol. Lett.* **2010**, *22*, 121–123. [[CrossRef](#)]
11. Petermann, K. External optical feedback phenomena in semiconductor-lasers. *IEEE J. Sel. Top. Quantum Electron.* **1995**, *1*, 480–489. [[CrossRef](#)]
12. Hwang, S.K.; Liu, J.M. Dynamical characteristics of an optically injected semiconductor laser. *Opt. Commun.* **2000**, *183*, 195–205. [[CrossRef](#)]
13. Gatare, I.; Sciamanna, M.; Buesa, J.; Thienpont, H.; Panajotov, K. Nonlinear dynamics accompanying polarization switching in vertical-cavity surface-emitting lasers with orthogonal optical injection. *Appl. Phys. Lett.* **2006**, *88*, 101106. [[CrossRef](#)]
14. Hong, Y.H.; Spencer, P.S.; Shore, K.A. Wideband chaos with time-delay concealment in vertical-cavity surface-emitting lasers with optical feedback and injection. *IEEE J. Quantum Electron.* **2014**, *50*, 236–242. [[CrossRef](#)]
15. Zhong, Z.Q.; Wu, Z.M.; Xia, G.Q. Experimental investigation on the time-delay signature of chaotic output from a 1550 nm VCSEL subject to FBG feedback. *Photon. Res.* **2017**, *5*, 6–10. [[CrossRef](#)]
16. Chen, J.J.; Li, C.X.; Mu, X.L.; Li, L.F.; Duan, Y.N. Time-delay signature suppression of polarization-resolved wideband chaos in VCSELs with dual-path chaotic optical injections. *Appl. Opt.* **2020**, *59*, 7217–7224. [[CrossRef](#)]
17. Zhao, A.; Jiang, N.; Zhang, Y.Q.; Peng, J.F.; Liu, S.Q.; Qiu, K.; Deng, M.L.; Zhang, Q.W. Semiconductor laser-based multi-channel wideband chaos generation using optoelectronic hybrid feedback and parallel filtering. *J. Lightwave Technol.* **2022**, *40*, 751–761. [[CrossRef](#)]
18. Chan, S.C.; Liu, J.M. Tunable narrow-linewidth photonic microwave generation using semiconductor laser dynamics. *IEEE J. Sel. Top. Quantum Electron.* **2004**, *10*, 1025–1032. [[CrossRef](#)]
19. Qi, X.Q.; Liu, J.M. Photonic microwave applications of the dynamics of semiconductor lasers. *IEEE J. Sel. Top. Quantum Electron.* **2011**, *17*, 1198–1211. [[CrossRef](#)]
20. Huang, Y.; Zhou, P.; Li, N.Q. Broad tunable photonic microwave generation in an optically pumped spin-VCSEL with optical feedback stabilization. *Opt. Lett.* **2021**, *46*, 3147–3150. [[CrossRef](#)]
21. Uchida, A.; Amano, K.; Inoue, M.; Hirano, K.; Naito, S.; Someya, H.; Oowada, I.; Kurashige, T.; Shiki, M.; Yoshimori, S.; et al. Fast physical random bit generation with chaotic semiconductor lasers. *Nat. Photonics* **2008**, *2*, 728–732. [[CrossRef](#)]
22. Reidler, I.; Aviad, Y.; Rosenbluh, M.; Kanter, I. Ultrahigh-speed random number generation based on a chaotic semiconductor laser. *Phys. Rev. Lett.* **2009**, *103*, 024102. [[CrossRef](#)] [[PubMed](#)]

23. Argyris, A.; Syvridis, D.; Larger, L.; Annovazzi-Lodi, V.; Colet, P.; Fischer, I.; Garcia-Ojalvo, J.; Mirasso, C.R.; Pesquera, L.; Shore, K.A. Chaos-based communications at high bit rates using commercial fibre-optic links. *Nature* **2005**, *438*, 343–346. [[CrossRef](#)] [[PubMed](#)]
24. Wu, J.G.; Wu, Z.M.; Tang, X.; Fan, L.; Deng, W.; Xia, G.Q. Experimental demonstration of LD-based bidirectional fiber-optic chaos communication. *IEEE Photonics Technol. Lett.* **2013**, *25*, 587–590. [[CrossRef](#)]
25. Lin, F.Y.; Liu, J.M. Diverse waveform generation using semiconductor lasers for radar and microwave applications. *IEEE J. Quantum Electron.* **2004**, *40*, 682–689. [[CrossRef](#)]
26. Lin, F.Y.; Liu, J.M. Chaotic lidar. *IEEE J. Sel. Top. Quantum Electron.* **2004**, *10*, 991–997. [[CrossRef](#)]
27. Zhong, D.Z.; Xu, G.L.; Luo, W.; Xiao, Z.Z. Real-time multi-target ranging based on chaotic polarization laser radars in the driveresponse VCSELS. *Opt. Express* **2017**, *25*, 21684–21704. [[CrossRef](#)]
28. Chen, Y.P.; Yi, L.L.; Ke, J.X.; Yang, Z.; Yang, Y.P.; Huang, L.Y.; Zhuge, Q.B.; Hu, W.S. Reservoir computing system with double optoelectronic feedback loops. *Opt. Express* **2019**, *27*, 27431–27440. [[CrossRef](#)]
29. Zhao, B.B.; Wang, X.G.; Zhang, J.C.; Wang, C. Relative intensity noise of a mid-infrared quantum cascade laser: Insensitivity to optical feedback. *Opt. Express* **2019**, *27*, 26639–26647. [[CrossRef](#)]
30. Zhao, B.B.; Wang, X.G.; Wang, C. Strong optical feedback stabilized quantum cascade laser. *ACS Photonics* **2020**, *7*, 1255–1261. [[CrossRef](#)]
31. Jumpertz, L.; Schires, K.; Carras, M.; Sciamanna, M.; Grillot, F. Chaotic light at mid-infrared wavelength. *Light Sci. Appl.* **2016**, *5*, e16088. [[CrossRef](#)] [[PubMed](#)]
32. Spitz, O.; Wu, J.G.; Carras, M.; Wong, C.W.; Grillot, F. Low-frequency fluctuations of a mid-infrared quantum cascade laser operating at cryogenic temperatures. *Laser Phys. Lett.* **2018**, *15*, 116201. [[CrossRef](#)]
33. Han, H.; Cheng, X.M.; Jia, Z.W.; Shore, K.A. Nonlinear dynamics of interband cascade laser subjected to optical feedback. *Photonics* **2021**, *8*, 366. [[CrossRef](#)]
34. Deng, Y.; Fan, Z.F.; Zhao, B.B.; Wang, X.G.; Zhao, S.Y.; Wu, J.G.; Grillot, F.; Wang, C. Mid-infrared hyperchaos of interband cascade lasers. *Light Sci. Appl.* **2022**, *11*, 7. [[CrossRef](#)]
35. Wolf, A. Wolf Lyapunov Exponent Estimation from a Time Series. MATLAB Central File Exchange. Available online: <https://www.mathworks.com/matlabcentral/fileexchange/48084-wolf-lyapunov-exponent-estimation-from-a-time-series> (accessed on 10 January 2022).
36. Wolf, A.; Swift, J.B.; Swinney, H.L.; Vastano, J.A. Determining Lyapunov exponents from a time-series. *Phys. D* **1985**, *16*, 285–317. [[CrossRef](#)]
37. Ott, E. *Chaos in Dynamical Systems*; Cambridge University: Cambridge, UK, 2002.
38. Sprott, J.C. *Chaos and Time-Series Analysis*; Oxford University: New York, NY, USA, 2003.
39. Matsumoto, T.; Chua, L.O.; Kobayashi, K. Hyperchaos: Laboratory experiment and numerical confirmation. *IEEE Trans. Circuits Syst.* **1986**, *33*, 1143–1147. [[CrossRef](#)]
40. Ferre, S.; Jumpertz, L.; Carras, M.; Ferreira, R.; Grillot, F. Beam shaping in high-power broad-area quantum cascade lasers using optical feedback. *Sci. Rep.* **2017**, *7*, 44284. [[CrossRef](#)]